ACS Catalysis

Research Article

Cite This: ACS Catal. 2019, 9, 7535−7547

pubs.acs.org/acscatalysis

Origin of the Selectivity and Activity in the Rhodium-Catalyzed Asymmetric Hydrogenation Using Supramolecular Ligands

Julien Daubignard,[†] Martin Lutz,[‡] Remko J. Detz,[†] Bas de Bruin,[†] and Joost N. H. Reek*[,†]

[†]Van't Hoff Institute for Molecular Sciences, University of Amsterdam, Science Park 904, Amsterdam 1098 XH, Netherlands

[‡]Crystal and Structural Chemistry Bijvoet Center for Biomolecular Research, Utrecht University, Padualaan 8, Utrecht 3584 CH, Netherlands

Supporting Information

ABSTRACT: The reaction mechanism of the asymmetric hydrogenation of functionalized alkenes catalyzed by a supramolecular rhodium complex has been investigated. In-depth NMR analysis combined with X-ray crystal structure determination show that hydrogen bonds are formed between the catalyst and the substrate in the early stages of the mechanism. Detailed kinetic data obtained from UV−vis stopped-flow experiments and gas-uptake experiments confirm that the hydrogen bonds are playing a crucial role in the mechanism. A complete DFT study of the various competitive paths of the reaction mechanism allowed us to identify how these hydrogen bonds are involved in the determining steps of the reaction.

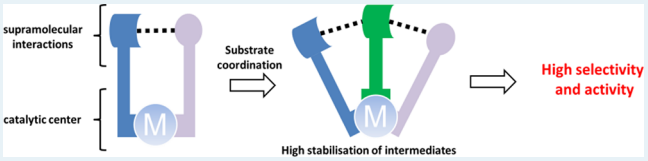

KEYWORDS: *asymmetric hydrogenation, rhodium, supramolecular interactions, hydrogen bond*

INTRODUCTION

The asymmetric hydrogenation of olefins is a powerful synthetic method for the preparation of chemicals, especially in the fields of agrochemicals, fragrances, and pharmaceuticals.[1−7] The interest of the industry for this reaction lies in the high atom economy, high reactivity, and, most importantly, the excellent enantiopurity of the products that are formed.[8] For this reason, academic and industrial research is strongly focused on the development of new catalysts that can supply a high degree of enantiopurity of the product and display high rates in the hydrogenation reaction. The field of asymmetric hydrogenation started with the pioneering work of Horner and Knowles demonstrating that a chiral version of the Wilkinson catalyst enabled enantioselective hydrogenation reactions, though with low enantiomeric excess at that time.[9,10] A breakthrough was reported independently by Kagan and Knowles, in which chiral bidentate phosphine ligands were used giving significant selectivity (up to 70% ee), opening the way for the design of new catalysts.[11−13] Numerous bidentate chelating phosphine ligands have been reported ever since and have been demonstrated to be selective in the hydrogenation of a variety of substrates. The success of bidentate ligands implied that such chelation of the ligand is a prerequisite to induce high enantioselectivity.[14−21] The working hypothesis was that the chelation of the ligand confers a high rigidity to the chiral environment around the metal center, leading to a high facial discrimination of the prochiral olefin. Among these chelating ligands, BINAP (developed by Noyori) stands out, and it is considered as one of the most important ligands in transition metal catalysis.[22] Interestingly, monodentate BINOL-based ligands, using the same chiral scaffold, also result in a rhodium catalyst that displays high enantioselectivity, revealing that high rigidity and chelation of the ligand is not essential. It was discovered by independent research groups that monophosphites,[23−25] monophosphonites,[26,27] and monophosphoramidites[28−30] are excellent ligands for rhodium-catalyzed asymmetric hydrogenation.[31−33] For this class of ligands, bulky substituents on the phosphorus atom are important to limit the rotation of the ligands around the axis phosphorus−metal.[34]

Next to ligand development, the mechanism of the asymmetric hydrogenation reaction has been widely studied, and the most important key steps of the reaction have been identified. The first important mechanistic findings were reported by Brown[35−39] and Halpern,[40−43] who studied rhodium complexes based on bidentate C_2-symmetric diphosphines. They reported the *unsaturated mechanism*, in which the substrate coordinates first to the catalyst, followed by oxidative addition of hydrogen. Halpern showed in a detailed investigation that the difference in energy between the two catalyst−substrate adducts (major/minor concept) is not responsible for the observed enantioselectivity. Instead, the minor adduct is the intermediate that reacts fast with molecular hydrogen to give the major product of the reaction. This mechanistic concept is known as the "anti-lock-and-key mechanism" or the Halpern mechanism. These results were later supported by computational studies reported by Felgus and Landis.[44−46] Although this was a leading concept for years, it was shown that it does not apply for all catalytic systems. Twenty years after the Halpern mechanism, a *lock-and-key* mechanism was reported for rhodium complexes based on C_2-symmetric bidentate ligands[47] and C_1-symmetric bidentate

Received: May 2, 2019
Revised: June 18, 2019
Published: July 12, 2019

DOI: 10.1021/acscatal.9b01809
ACS Catal. 2019, 9, 7535−7547

ligands.[48−53] In this mechanism, the major catalyst−substrate adduct is the one reacting with hydrogen to give the final product of the reaction. More recently, the in-depth studies of Gridnev and Imamoto have demonstrated that some catalytic systems can follow a *hydride mechanism* in which the catalyst activates molecular hydrogen prior to substrate coordination.[54−59] Also, they report the reversibility of all the possible steps prior to the irreversible hydride migration and finally conclude that the enantioselection is determined at the stage of recoordination of the prochiral olefin in a nonchelating octahedral Rh(III) complex prior to the insertion.

The rational design of new and selective catalysts based on mechanistic consideration is still challenging,[60−63] and therefore high-throughput screening remains the dominant strategy to identify new catalysts. In this context, monodentate ligands have demonstrated their value, as their synthesis is generally more easy to adapt for combinatorial approaches.[24,64−68] The use of supramolecular bidentate ligands formed by self-assembly through noncovalent interactions has more recently been reported and is now a frequently applied strategy leading to excellent selectivities, regularly achieving higher selectivities than the classic catalysts.[69−80] In some cases,[81−84] the success of such approaches has been ascribed to crucial noncovalent interactions between the catalyst and the substrate, and to date, only few reports have been released on such systems for the catalytic hydrogenation of alkenes.[75] Interestingly, the importance of such supramolecular interactions between the substrate and the catalyst in the reaction of asymmetric hydrogenation was already proposed in some of the first developed bidentate ligands.[84−88]

Complex $[Rh(\mathbf{L_1})(\mathbf{L_2})(cod)]BF_4$ (complex **1**, Figure 1) has recently been introduced as a new supramolecular catalyst

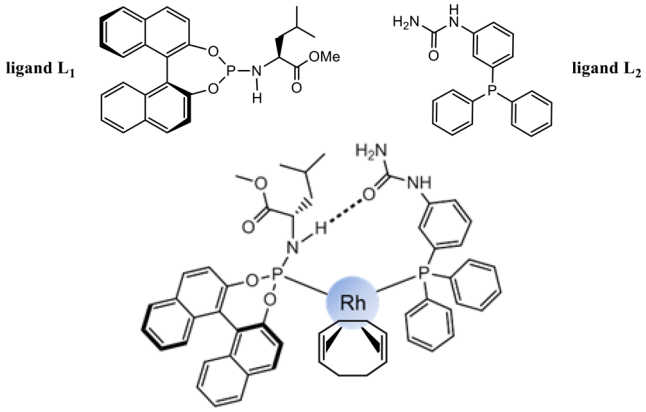

Figure 1. Top: monophosphorus ligand building blocks used for the formation of supramolecular complex **1**. Bottom: complex **1** $[Rh(\mathbf{L_1})(\mathbf{L_2})(cod)]BF_4$ (cod = 1,5-cyclooctadiene).

bearing a heterobidentate ligand formed by self-assembly through a single hydrogen bond between the NH group of a phosphoramidite and the urea carbonyl of a urea-functionalized phosphine (Figure 1).[89] This complex affords the highest enantioselectivity (>99% ee) reported up to now for the hydrogenation of methyl 2-hydroxymethacrylate (and several of its derivatives, Table 1), which is a precursor of the so-called "Roche ester", an important intermediate in the preparation of several biologically active compounds (**S1**, Table 1).[90]

Table 1. Asymmetric Hydrogenation of Methyl-2-hydroxymethylacrylate Derivatives S1−S6 Using $[Rh(\mathbf{L_1})(\mathbf{L_2})(cod)]BF_4$ (1) as Catalyst[a]

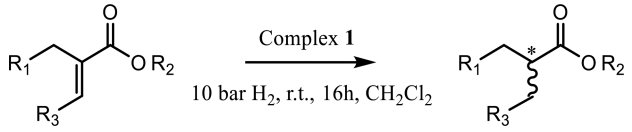

substrate	R_1	R_2	R_3	conversion (%)	ee (%)
S1[b]	OH	Me	H	100	99
S2[b]	OH	*t*Bu	H	100	99
S3[b]	OH	Me	Ph (E)	83	98[c] (*S*)
S4	OMe	Me	Ph	67	25 (*S*)
S5	H	Me	Ph	55	7
S6	OH	Me	Ph (Z)	80	74

[a][complex **1**] = 0.2 mM; [substrate] = 0.1 M; solvent, CH_2Cl_2; reaction performed at 10 bar H_2 pressure at 25 °C for 16 h. [b]Results previously reported in ref 89. [c]ee obtained for this substrate varies between 96% and 99%.

In this paper, we report how supramolecular interactions are involved in the mechanism of the asymmetric hydrogenation reaction, leading to very high enantioselectivity. An in-depth mechanistic investigation demonstrates that the mechanism operates via a *lock-and-key* mechanism.[91] Secondary interactions between the substrate and the catalyst were identified during the early stage of the reaction and are involved in the discrimination of the prochiral faces of the substrate. Finally, computational studies confirm the crucial role of the secondary interactions between the substrate and the catalyst throughout the whole reaction pathway. This insight in the mechanism provides handles to use supramolecular interactions as a tool in the design of new catalysts for the asymmetric hydrogenation.

RESULTS

This paper consist of three parts: (1) the identification of intermediates of the catalytic cycle by the use of different analytical techniques (multinuclear NMR, UV−vis, X-ray crystal structure determination); (2) discussion of the kinetics of the reaction, evaluated by means of stopped-flow UV−vis methods and gas-uptake experiments; and (3) an extensive DFT study that shows how the hydrogen bonds between the substrate and the catalyst are involved along the reaction pathway and are responsible for the high selectivity observed.

Characterization of the Precatalyst and Solvate Species. Metal complex **1** ($[Rh(\mathbf{L_1})(\mathbf{L_2})(cod)]BF_4$) as the precatalyst of the reaction was first characterized. Mixing of the ligands and the rhodium precursor reveals the quantitative formation of the complex as indicated by the ^{31}P NMR spectrum (δ P^1 132.05 ppm, $^1J_{P,Rh}$ = 242.3 Hz, $^2J_{P,P'}$ = 31 Hz; δ P^2 34.03 ppm, $^1J_{P,Rh}$ = 149.5 Hz, $^2J_{P,P'}$ = 31 Hz).[89] The supramolecular interaction between the ligands was further studied by 2D $^1H-^1H$ COSY NMR showing a strong downfield shifted NH group (δ = 6.24 ppm).[92] This value was compared to the shift of the NH group in the analogue complex based on triphenylphosphine, in which this group is not hydrogen bonded.[93] The large difference between the chemical shift of the NH groups of the two different complexes ($\Delta\delta$ = 1.95 ppm) indicates the presence of the NH−urea hydrogen bond.[94] Single crystals of complex **1** were obtained by layering pentane onto a solution of the complex. The solid

DOI: 10.1021/acscatal.9b01809
ACS Catal. 2019, 9, 7535−7547

state structure obtained from X-ray analysis at low temperature reveals the anticipated hydrogen bonding (Figure 2).

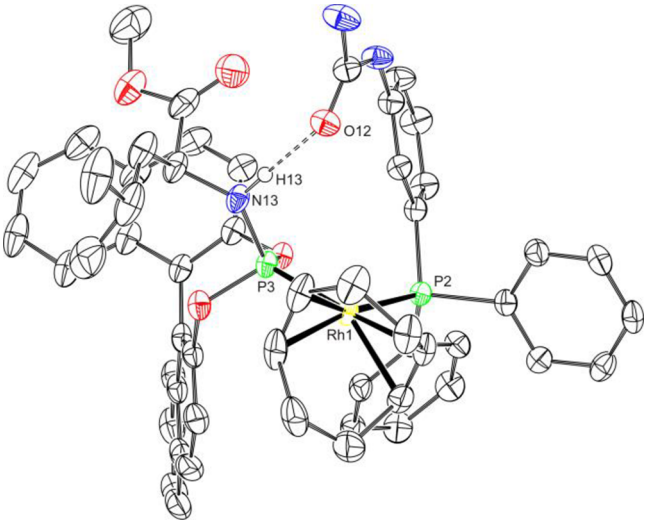

Figure 2. ORTEP view of the X-ray crystal structure of complex **1** ([Rh($\mathbf{L}_1$)($\mathbf{L}_2$)(cod)]BF_4; cod= 1,5-cyclooctadiene). The anion, all C−H hydrogen atoms, and solvent molecules have been omitted for clarity. The hydrogen bond between the two ligands has a length of 2.05(3) Å.

A solution of complex **1** in CD_2Cl_2 was hydrogenated under 5 bar for 2 h at −90 °C. The hydrogenation of the coordinating diene was monitored by ^{1}H NMR until complete disappearance of the precatalyst was observed. The sample was then degassed by four freeze−pump−thaw cycles, after which a ^{31}P NMR spectrum was recorded. At low concentration (C = 0.015 M), a mixture of several species with broad signals was observed. The spectrum did not sharpen at lower temperature in the range 293−183 K indicating the formation of undefined solvate species at low concentration, most likely being monomeric solvate species (solvate complex **2**). When 10 equiv of acetonitrile-d_3 was added to a solution of solvate complex **2**, a new major species was observed in solution by ^{31}P NMR (δ P^1 140.91 ppm, $^1J_{P,Rh}$ = 267.1 Hz, $^2J_{P,P'}$ = 59.7 Hz; δ P^2 50.6 ppm, $^1J_{P,Rh}$ = 178.0 Hz, $^2J_{P,P'}$ = 59.7 Hz). A series of NMR experiments (^{31}P NMR, 2D COSY ^{1}H−^{1}H NMR) demonstrated that the monomeric acetonitrile solvate complex **2′** had formed.[92] In the ^{1}H NMR spectrum a downfield chemical shift of the NH group of the phosphoramidite at 5.76 ppm was observed, indicating that also in the monomeric acetonitrile complex **2′** a hydrogen bond is formed between the two ligands. This is further supported by the X-ray crystal structure of the acetonitrile complex **2′** (Figure 3).

Characterization of Substrate−Catalyst Complexes. When 3 equiv of (E)-methyl 2-(hydroxymethyl)-3-phenyl acrylate (substrate **S3**, Table 1) was added to a solution of solvate complex **2**, the ^{31}P NMR spectrum revealed the formation of a new species, appearing as a set of doublet of doublets (Figure 4, δ P^1 133.22 ppm, $^1J_{P,Rh}$ = 308.2 Hz, $^2J_{P,P'}$ = 37.1 Hz; δ P^2 47.67 ppm, $^1J_{P,Rh}$ = 205.1 Hz, $^2J_{P,P'}$ = 37.1 Hz). On the basis of a ^{13}C NMR experiment, we identified the new species as a catalyst−substrate complex **3** in which the carbonyl group of the substrate is coordinated to the metal center.[92] The coordination of the alkene group could not be established from the complicated ^{13}C NMR/HSQC spectra.

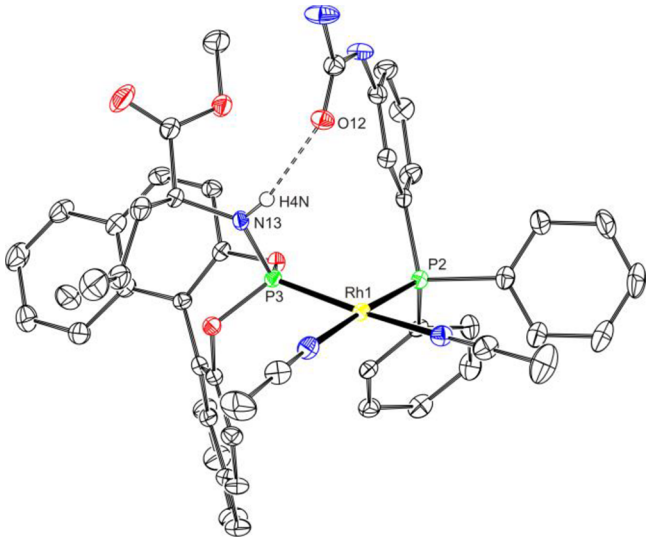

Figure 3. ORTEP view of the X-ray crystal structure of the acetonitrile-d^3 complex **2′** ([Rh($\mathbf{L}_1$)($\mathbf{L}_2$)(acetonitrile)$_2$]BF_4). The anions and all C−H hydrogen atoms have been omitted for clarity. The hydrogen bond between the two ligands has a length of 2.24(3) Å.

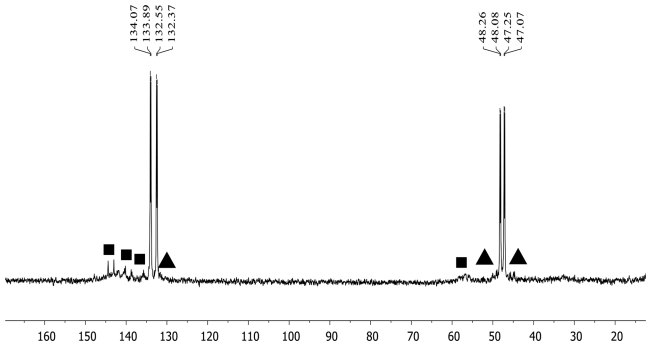

Figure 4. ^{31}P NMR spectrum after the addition of 3 equiv of substrate **S3** to solvate complex **2** in CD_2Cl_2 (162 MHz): ■, solvate complex undefined species; ▲, minor diastereomers.

However, the ^{1}H NMR/2D ^{1}H−^{1}H COSY NMR experiments identified the methylene group of the coordinated substrate as a set of diastereotopic protons (see the experimental sections in the SI).

The strong desymmetrization of the methylene group can only be attributed to coordination of the double bond adjacent to the methylene group. Therefore, the NMR spectra confirm the formation of a catalyst−substrate adduct in solution in which both the carbonyl group of the substrate and the double bond are coordinated to the metal center. Since we could not determine the exact coordination mode of the catalyst−substrate complexes (Re or Si face coordinated), we calculated by DFT the free energy of the four possible diastereoisomers that can be generated after coordination of the prochiral substrate **S3** on the C_1-symmetric catalyst. Interestingly, the diastereoisomer with the lowest energy (Figure 5, structure **3a**) features a unique structure in which two hydrogen bonds are formed between the catalyst and the substrate. One hydrogen bond is formed between the NH of the phosphoramidite and the oxygen of the hydroxyl group of the substrate, and the second one is formed between the carbonyl of the urea group on the phosphine and the proton of the hydroxyl group of the

DOI: 10.1021/acscatal.9b01809
ACS Catal. 2019, 9, 7535−7547

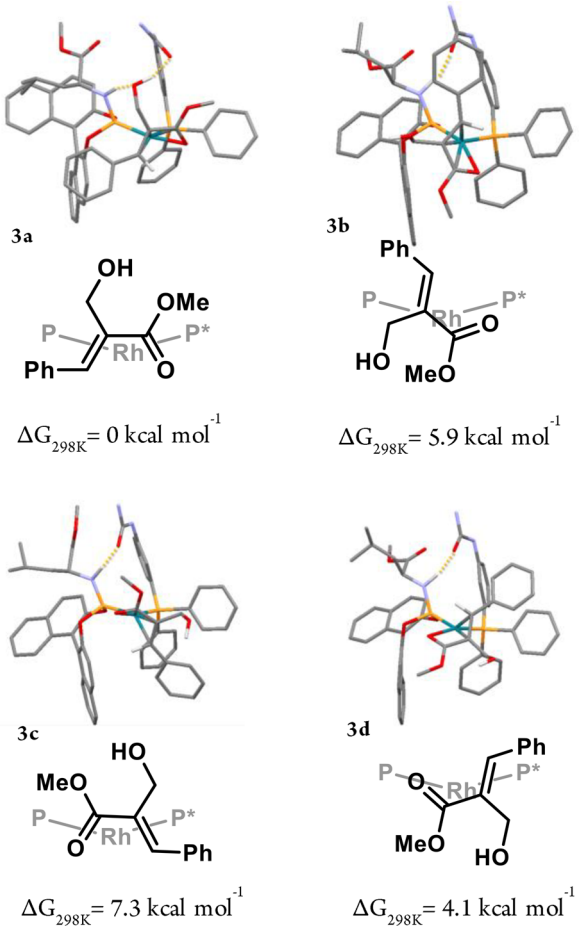

Figure 5. Calculated structures of the four possible catalyst–substrate complexes **3** (optimized with DFT, BP86, def2-TZVP/disp3).[92] Most hydrogen atoms on the complexes have been removed in the figure for clarity (except the hydrogen atoms involved in the H-bond, the hydrogen atom of the hydroxyl group, and the hydrogen atom of the alkene). When no hydrogen bonds are present between the substrate and the catalyst in **3a**, the relative energy calculated was found to be ΔG_{298K} = +5.5 kcal mol^{-1}. In the chemdraw structure P = **L1** and P* = **L2**.

substrate. As a consequence, the hydroxyl group of the substrate is inserted between the functional groups of the two ligands resulting in a highly stabilized substrate–catalyst complex through supramolecular interactions.[95] Also, we calculated the energy of diastereomer **3a** of the same conformation but without the H-bond (hydroxyl group pointing out). This complex was found to be 5.45 kcal mol^{-1} higher in energy than diastereomer **3a**. The formation of a different hydrogen bond interaction in substrate–catalyst complex **3** was further supported by NMR spectroscopy. The NH group of the phosphoramidite ligands in substrate–catalyst complex **3** was further downfield shifted (δ = 5.54 ppm) compared to the same hydrogen bonded NH in complex **2** (δ = 6.24 ppm).

Upon hydrogenation of the chelate complex **3a**, no late intermediates of the reaction mechanism could be observed by high pressure (HP) NMR experiments, even at low temperatures. After completion of the hydrogenation, the product of the reaction is obtained with an enantiomeric excess of 98% in favor of the *S*-enantiomer, as indicated by GC analysis.[96] Importantly, in the substrate–catalyst complex **3a**, the substrate is coordinated on its prochiral Si face, yielding the *S*-enantiomer of the product, as was observed experimentally. These observations are in line with a lock-and-key mechanism in which diastereomer **3a** is the most stable and the most reactive intermediate in the follow-up steps in the hydrogen reaction.

Study of Analogue Substrates. To further study the influence of the supramolecular interaction in the catalyst–substrate complex **3**, comparative experiments were carried out with substrate **S4**, lacking the hydrogen bond donor (entry 4, Table 1). Under standard conditions,[97] the hydrogenation of substrate **S4** gives an enantiomeric excess of 25%, showing a drastic decrease in the enantioselectivity of the reaction when compared to the hydrogenation of the substrate bearing a H-bond donor group (substrate **S3**, 98% ee). To form the substrate-adduct of the complex, 3 equiv of substrate **S4** was added to the solvate complex **2**, but this did not lead to the formation of well-defined species according to the ^{31}P NMR spectrum, most likely due to low binding constant of substrate **S4**. Upon addition of 12 equiv of substrate **S4** to a 0.01 M solution of solvate complex **2**, two doublets of doublets were observed in ^{31}P NMR indicating the formation of one diastereomer in solution (δ P^1 133.09 ppm, $^1J_{P,Rh}$ = 308.2 Hz, $^2J_{P,P'}$ = 37.0 Hz; δ P^2 48.16 ppm, $^1J_{P,Rh}$ = 205.1 Hz, $^2J_{P,P'}$ = 37.0 Hz) (Figure 6).

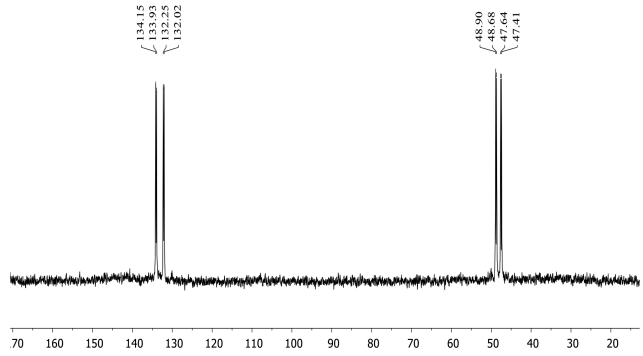

Figure 6. ^{31}P NMR spectrum after addition of 12 equiv of substrate **S4** to solvate complex **2** in CD_2Cl_2 (162 MHz).

Even though the chemical shifts and coupling constants observed in the ^{31}P NMR signals for the catalyst–substrate **S4** complex are very similar to those observed for catalyst–substrate **S3** complex, the exact coordination mode of the substrate could not be determined from the NMR analysis (pro-*S* or pro-*R*). Therefore, we calculated the possible diastereomers that can be formed upon coordination of the prochiral double bond to the rhodium center (Figure 7). As can be seen from Figure 7, no hydrogen bonds between the catalyst and the substrate are present in the optimized structures of the four diastereomers. Interestingly, the diastereomer of lowest energy (structure **4a**, Figure 7) has the same configuration as **3a**, corresponding to the coordination of the pro-*S* face to the metal center.

The stoichiometric hydrogenation of catalyst–substrate **4a** provides the *S*-product.[98] Therefore, in the mechanism of hydrogenation of substrate **S3** and **S4**, the major diastereomer observed in solution reacts with hydrogen to provide the product of the reaction (*S*-enantiomer). Even though the hydrogen bond does not have a large effect on the relative energies of the substrate complexes, still a large difference in

DOI: 10.1021/acscatal.9b01809
ACS Catal. 2019, 9, 7535–7547

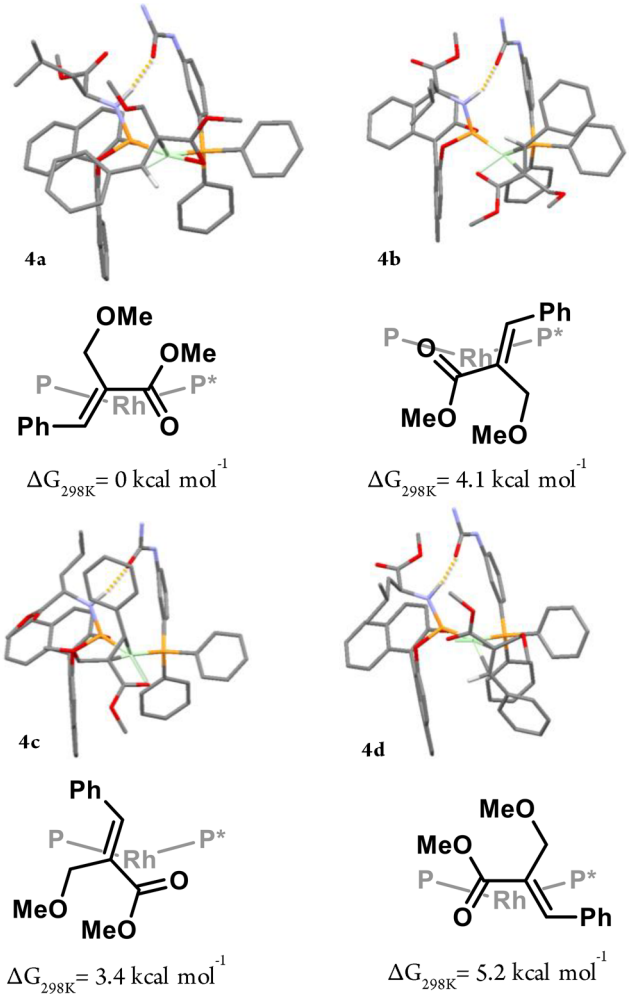

Figure 7. Calculated structures of the 4 possible catalyst−substrate complexes **4** (optimized with DFT at the BP86 level, def2-TZVP/disp3).[92] All hydrogen atoms on the catalyst have been omitted for clarity (except the hydrogen atoms involved in the hydrogen bond between the two ligands). In the chemdraw structure P = **L1** and P* = **L2**.

enantioselective conversion is observed between substrate **S3** and **S4**. Upon pressurizing a solution of the solvate complex **2** under hydrogen (10 bar) under otherwise standard conditions, no hydrides species were detected by NMR, even at very low temperature (−90 °C). This implies that the mechanism does not follow the classical dihydride pathway proposed by Gridnev and co-workers, but most likely the unsaturated pathway. As demonstrated by Gridnev, the possible crossovers between the *unsaturated pathway* and the *dihydride* pathways (and the reversibility of the steps inherent to these two paths) involve the existence of a common intermediate that connects the two routes in the late stages of the mechanism.[99]

Evaluation of Substrate Coordination (S3, S4) to Coordination Complex 2 by UV−vis. The equilibrium defined in Scheme 1 (substrate **S3**) and Scheme 2 (substrate **S4**) has been studied by means of UV−vis spectroscopy.[92] The binding constants of substrate **S3** and **S4** to the solvate complex **2** in dichloromethane have been determined by titration experiments, and these were found to be 137 and 62 M^{-1}, respectively. These values are in accordance with values found in the literature (Halpern found a binding constant of 3 M^{-1} for the association of methyl acrylate to a similar

Scheme 1. Coordination of Substrate S3 to Complex 2 Leading to Complex 3, As Identified by NMR, Leading to Formation of the *S*-Product after Reaction with Molecular Hydrogen

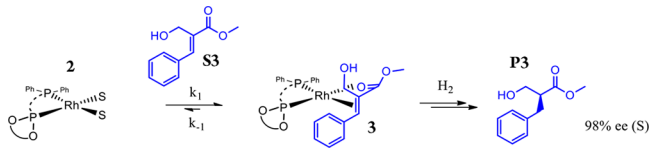

Scheme 2. Binding of Substrate S4 to Catalyst 2 and Subsequent Stoichiometric Hydrogenation To Form the *S*-Product P4

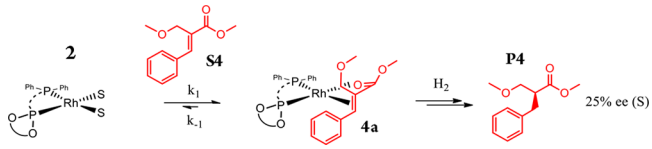

bisphosphine-based solvate complex in methanol).[40] Interestingly, the difference in free energy between the binding of the substrate that can (substrate **S3**) and cannot (substrate **S4**) donate a hydrogen bond is in the typical order of magnitude of a hydrogen bond ($\Delta\Delta G = \pm 2.2$ kcal mol^{-1}). The difference in energy is in line with the existence of a secondary interaction in structure **3a**, as was observed computationally.

The rates of association of substrate **S3** and **S4** on solvate complex **2** (Schemes 1 and 2) were studied using stopped-flow time-resolved UV−vis spectroscopy. A solution of solvate complex **2** in CH_2Cl_2 ($C_{Rh} = 2.5.10^{-4}$ M) and a solution of an excess of substrate ($C_{sub} = 3.75.10^{-2}$ M) were rapidly mixed in a stopped-flow spectrophotometer, and the change in absorbance (λ = 390 nm) was recorded until the equilibrium was reached.[92] The measurements were performed under pseudo-first-order conditions by using a 150-fold substrate excess. Under these conditions, the rate law of the substrate coordination can be simplified as

$$\frac{d[\mathbf{3}]}{dt} = k_{obs}[\mathbf{2}] \quad (1)$$

with $k_{obs} = k_1[\mathbf{S3}]$.

The coordination reaction is initially fast (at 1/3 in the first 10 s), but the equilibrium is reached only after 10 min. A pseudo-first-order rate is observed only during the first seconds of the reaction.[92]

Dependency of the Enantiomeric Excess on the Hydrogen Pressure. The influence of H_2 pressure on the enantioselectivity provides indirect information on the mechanism.[100−103] For this reason, we studied the influence of the hydrogen pressure in the range 1−40 bar on the enantioselectivity of the hydrogenation reaction of substrates **S3**, **S4**, and **S5** and by using complex **1** as the catalyst (Figure 8).[104]

Remarkably, the enantioselectivity obtained in the hydrogenation of substrate **S3** is independent of the hydrogen pressure while the enantioselectivity of the hydrogenation of substrates **S4** and **S5** is highly influenced by the hydrogen pressure. Within the range 1−10 bar, the enantiomeric excess of the hydrogenation of substrate **S4** drops from 86% to 25% while the enantiomeric excess of the hydrogenation of **S3** is very high between 1 and 40 bar. These observations can be

DOI: 10.1021/acscatal.9b01809
ACS Catal. 2019, 9, 7535−7547

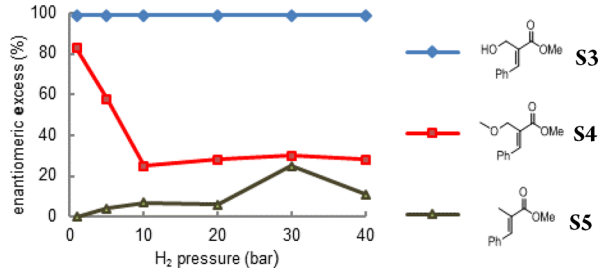

Figure 8. Dependency of the enantiomeric excess on the hydrogen pressure for substrates **S3**, **S4**, and **S5** catalyzed by complex **1**. Conditions: Rh/substrate = 1:100, c_0 (substrate) = 0.1 M, 1−40 bar H_2, CH_2Cl_2, r.t., 18 h.

explained by two mechanistic hypotheses: (1) Substrates **S3** and **S4** are following the same reaction pathway (*anti-lock-and-key* or *lock-and-key*), but in the case of substrate **S3**, the secondary interaction makes the enantioselection less dependent on the hydrogen pressure. (2) The secondary interaction induces a switch in the mechanisms of substrates **S3** and **S4** (*lock-and-key* for substrate **S3**, *anti-lock-and-key* for substrate **S4**). To distinguish between these different hypotheses, we further investigated the kinetics of the hydrogenation of substrates **S3** and **S4**.

Analysis of the Kinetics by Gas-Uptake Experiments. We studied the kinetics of the hydrogenation reaction of substrate **S3** by complex **1** in more detail. Monitoring the reaction progress by the gas uptake for experiments with different initial substrate concentrations reveals a positive-order dependency of the reaction rate (TOF in mol mol^{-1} h^{-1}) on the substrate concentration (Table 2 and Figure 9). Also,

Table 2. Gas-Uptake Experiments Performed on the Hydrogenation of Substrate S3 by Complex 1 and Corresponding TOF[a]

entry	C_0 (M)	$p(H_2)$ (bar)	conversion [%]	TOF[b]	ee [%]
1	0.1	10	99.5	671	99.9
2	0.15	10	98	834	99.4
3	0.2	10	98	875	95.5
4	0.25	10	95	924	99.1
5	0.2	20	94	1620	98
6	0.2	30	87	2498	98
7	0.2	40	100	3398	99

[a]Reagents and conditions: [Rh] = 0.2 mM; solvent (8 mL), CH_2Cl_2; at 298 K for 20 h. [b]TOF in mol mol^{-1} h^{-1} calculated at 15% conversion from the slope of the gas curves.

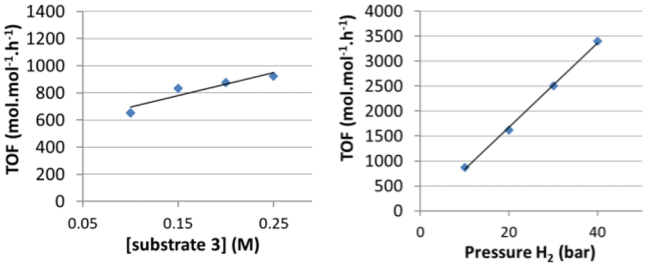

Figure 9. Left: TOF (in mol mol^{-1} h^{-1}, calculated at 15% conversion) as a function of the substrate **S3** concentration. Right: TOF (in mol mol^{-1} h^{-1}, calculated at 15% conversion) as a function of the dihydrogen pressure observed for substrate **S3**.

experiments performed at different pressures of hydrogen revealed a positive dependency of the TOF on the hydrogen concentration (Table 2 and Figure 9). The comparison of the TOF as a function of substrate concentration and the TOF as a function of the H_2 pressure (Figure 9) clearly shows that the reaction has a higher order in the hydrogen concentration than in the substrate concentration. Both *in situ* HP NMR spectroscopy and gas-uptake experiments are in accordance with a rate-determining step late in the catalytic cycle, being either oxidative addition or hydride migration.[105]

We performed the same series of experiments with substrate **S4**, the substrate that cannot form hydrogen bonds with the catalyst. The rate of the reaction was much lower than for substrate **S3**. Therefore, the catalyst concentration had to be increased to from 0.2 to 1 mM to obtain suitable gas-uptake curves. The analysis of the TOF for different initial substrate concentrations reveals a zero-order dependency of the reaction rate on the substrate concentration and a positive-order dependency of the TOF on the hydrogen pressure (Table 3 and Figure 10).[106]

Table 3. Gas-Uptake Experiments Performed on the Hydrogenation of Substrate S4 by Complex 1 and Corresponding TOF[a]

entry	C_0 (M)	$p(H_2)$ (bar)	conversion [%]	TOF[b]	ee [%]
1	0.1	10	89	58	42
2	0.15	10	83	61	27
3	0.2	10	76	58	38
4	0.25	10	72	59	37
5	0.2	20	87	98	38
6	0.2	30	90	133	45
7	0.2	40	94	116	36

[a]Reagents and conditions: [Rh] = 1 mM; solvent (8 mL), CH_2Cl_2; at 298 K for 20 h. [b]TOF on mol mol^{-1} h^{-1} calculated at 15% conversion from the slope of the gas curves.

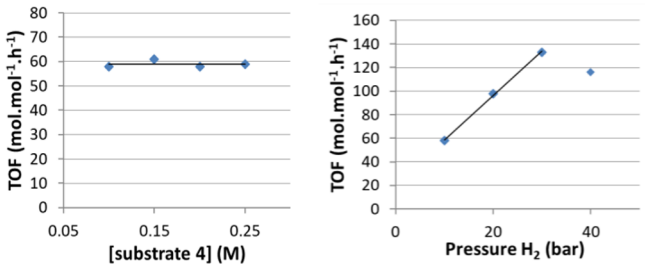

Figure 10. Left: TOF (in mol mol^{-1} h^{-1}, calculated at 15% conversion) as a function of the substrate **S4** concentration. Right: TOF (in mol mol^{-1} h^{-1}, calculated at 15% conversion) as a function of the dihydrogen pressure observed for substrate **S4**.

The Michaelis−Menten (MM) kinetic model has been used to describe the reaction rates of transition-metal-catalyzed reactions including hydrogenation[50] and hydroformylation.[107] In the asymmetric hydrogenation reaction following an unsaturated pathway, the system can be described by the reversible coordination of the alkene to the catalyst followed by the irreversible reaction of the catalyst−substrate complex with molecular hydrogen (Figure 11). As the current catalytic system displays such behavior, we used the MM kinetic model to further investigate the mechanism of hydrogenation of substrate **S3** and substrate **S4**. As product inhibition was

DOI: 10.1021/acscatal.9b01809
ACS Catal. 2019, 9, 7535−7547

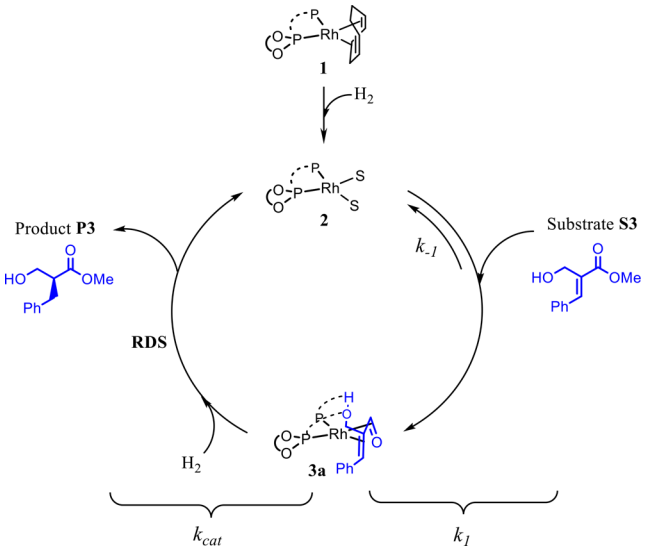

Figure 11. Proposed catalytic cycle for the asymmetric hydrogenation of substrate **S3**/**S4** using complex **1**.

observed in the gas-uptake experiments, the MM kinetic model with competitive product inhibition was used in this study (eq 2; V = reaction rate (in M h^{-1}), V_{max} = maximum reaction rate (in M h^{-1}), K_{MM} = Michaelis–Menten constant (in M), K_i = product inhibition constant (in M), [S] = substrate concentration (in M), and [P] = product concentration (in M)).

$$V = \frac{V_{max}[S]}{K_{MM} + [S] + \frac{K_{MM}}{K_i}[P]} \quad (2)$$

The combined data from gas-uptake experiments obtained for substrate **S3** as well as for substrate **S4** were fitted successfully to the MM rate equation (eq 2), giving the kinetic parameters of the reactions (Table 4).

Table 4. Kinetic Parameters Obtained from the Fitting of the Kinetic Data for Substrate S3 and Substrate S4 to the Michaelis–Menten Rate Equation with Competitive Product Inhibition

	substrate **S3**	substrate **S4**
V_{max} (M h^{-1})	0.38701	0.15815
K_{MM} (M)	0.04282	0.06002
K_i (M)	0.01449	0.00424

The maximum reaction rate (V_{max}) observed for substrate **S3** is higher than for substrate **S4**, in line with the analysis of the turnover frequencies at different initial substrate concentrations. Small values of K_{MM} in Table 4 indicate that most of the catalyst is present as the catalyst–substrate complex **3a** (or catalyst–substrate complex **4a** in the case of substrate **S4**), i.e., the resting state of the catalyst. Also the Michaelis–Menten constant K_{MM} observed for substrate **S3** is lower than for substrate **S4**, and therefore, substrate **S3** has a stronger affinity for the catalyst than substrate **S4**. This is in line with the binding constants measured for substrate **S3** and substrate **S4** (which are 137 and 62 M^{-1}, respectively) as well as with the coordination experiments.

At high substrate concentration (i.e., at the beginning of the reaction), the concentration of the intermediate complex **3a** is constant. Therefore, the quasi-steady-state approximation (QSSA) can be applied and allows for the estimation of the value of K_{MM}, given as

$$K_{MM} = \frac{k_{-1} + k_{cat}}{k_1} \quad (3)$$

From eq 3, we calculated the reaction rate constant of the reaction k_{cat} for substrates **S3** and **S4** using the values of k_1, k_{-1}, and K_{MM} calculated from the different kinetics and coordination experiments.[92] The values of k_{cat} for substrate **S3** and substrate **S4** are 0.616 and 0.401 s^{-1}, respectively (these values are in the same order as reported in the literature for the asymmetric hydrogenation using similar complexes and substrates).[40] Thus, the rate constant of the reaction k_{cat} for the hydrogenation of substrate **S3** is higher than for substrate **S4** suggesting a beneficial effect of the hydrogen bond between the catalyst and the substrate **S3** in the late stages of the catalytic cycle.

Also, under the standard conditions ([S] = 0.1 M, 10 bar H_2)

$$k_{cat} < k_1$$

Thus, for both substrates the rate-determining step of the reaction (RDS) is located at the late stages of the mechanism, i.e., after the coordination of the substrate. The RDS can be either the oxidative addition of H_2 to the square planar complex **3a** or the hydride migration step.

The combined experiments show that the reaction follows the unsaturated pathway, with the rate-limiting step late in the catalytic cycle. The hydrogen bond between the catalyst and the substrates not only influences the substrate coordination, but also leads to higher rates and higher enantioselectivity. To gain insight in the role of the hydrogen bond at the different stages of the catalytic cycle, we performed DFT calculations.

DFT-Calculated Reaction Pathways. Experimental studies suggest that the mechanism of the reaction is likely to follow an unsaturated mechanism under standard conditions (1–10 bar H_2). Also, in-depth kinetic studies disclosed that the rate-determining step of the reaction is located after the coordination of the substrate in the reaction mechanism. To unravel the mechanism of the reaction, we decided to take into account the various possible competitive pathways for the reaction: the *unsaturated pathway*, the *dihydride pathway*, and the more recently proposed *semidihydride pathway*. We calculated the potential energy profiles for these paths, and we found that the unsaturated pathway is the lowest in energy in the full energy landscape (see the Supporting Information).

Investigation of the Unsaturated Pathway. The coordination of the prochiral substrate to the C_1-symmetric solvate complex **1** can lead, in theory, to the formation of four diastereoisomers: two pro-*S* diastereomers and two pro-*R* diastereomers. As described in the Characterization of Substrate–Catalyst Complexes section, one of these diastereomers is stabilized by two hydrogen bonds between the substrate and the catalyst. We also computed the same diastereomer but without the H-bond stabilizing substrate–catalyst interaction revealing that this one was 5.45 kcal mol^{-1} higher in energy than the one stabilized by H-bonding (Figure 12). To understand if the H-bond stabilized diastereomer is the most active, we studied all the intermediates and transition states of the unsaturated pathways stemming from the same

DOI: 10.1021/acscatal.9b01809
ACS Catal. 2019, 9, 7535–7547

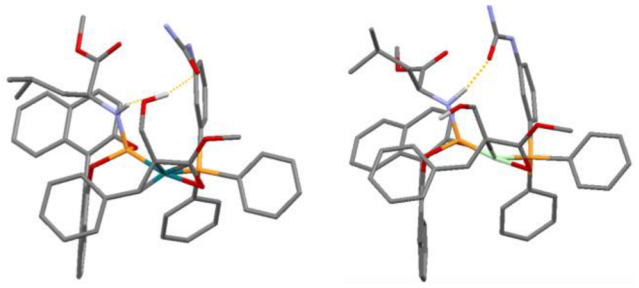

Figure 12. Calculated structures of the two major pro-*S* catalyst–substrate complexes, with and without H-bonding between the catalyst and the substrate (optimized with DFT, BP86, def2-TZVP/disp3). Hydrogen atoms on the catalyst have been removed for clarity, except the hydrogen atoms involved in the H-bonding.

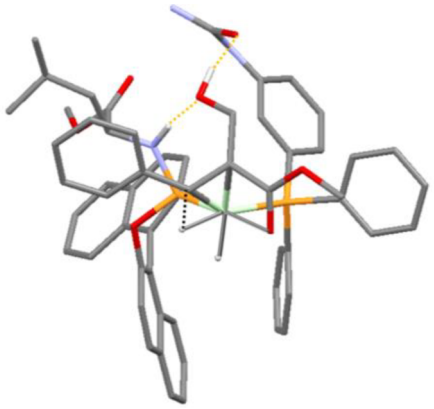

Figure 13. Optimized structure of the hydride migration transition state **TS3** (ΔG_{298K} = +20.9 kcal mol^{-1}/2, $\upsilon^{\ddagger}$ = 626.2*i* cm^{-1}). Hydrogen bonds are drawn in orange. The black dotted line represents the hydride insertion to form the alkyl hydride species **6**.

pro-*S* diastereoisomer, with and without hydrogen bond interactions (Figure 14).

We first computed the unsaturated pathway from the H-bond stabilized diastereoisomer **2** with **TS3** as the highest energy barrier (Figure 13) (black pathway, Figure 14). The presence of the hydrogen bond network on the upper face of the catalyst prevents the approach of the molecular hydrogen on this face, thus reducing the number of possible intermediates. In fact, the approach of hydrogen can only take place via the lower face of the catalyst (structure **3**) leading to σ-hydrogen complex **4**. Upon oxidative addition, the substrate must rotate to evolve into a dihydride octahedral complex. Due to the hydrogen bond interaction between the substrate and the catalyst, the clockwise rotation of the substrate is favored, thus forming the dihydride octahedral complex **5** via a low barrier transition state **TS1**. On the other hand, the rotation of the substrate in a counterclockwise manner is prevented by the interaction that pulls the substrate in the opposite direction, leading to a higher energy barrier **TS2** and reducing the number of possible pathways (purple path, Figure 14). The dihydride intermediate **5** undergoes hydride migration by a high energy barrier (**TS3**) leading to the alkylhydride species **6** (Figure 13). The reductive elimination (**TS4**) affords the complex solvate-product **7** in which the product is coordinated through the carbonyl and the hydroxyl groups to the complex.

To evaluate the importance of the hydrogen bonds in the pathway stemming from diastereoisomer **2**, we computed the unsaturated pathways from the same pro-*S* diastereomer that does not involve a secondary interaction between the substrate and the catalyst (structure **8**; for energy profile curves, see the Supporting Information). In this case, the upper face of the catalyst is less hindered, and the approach of molecular hydrogen can take place from both the upper face (red path, Figure 14) and the lower face (green and blue path, Figure 14). For each "non-H-bond" path, we have computed the σ-

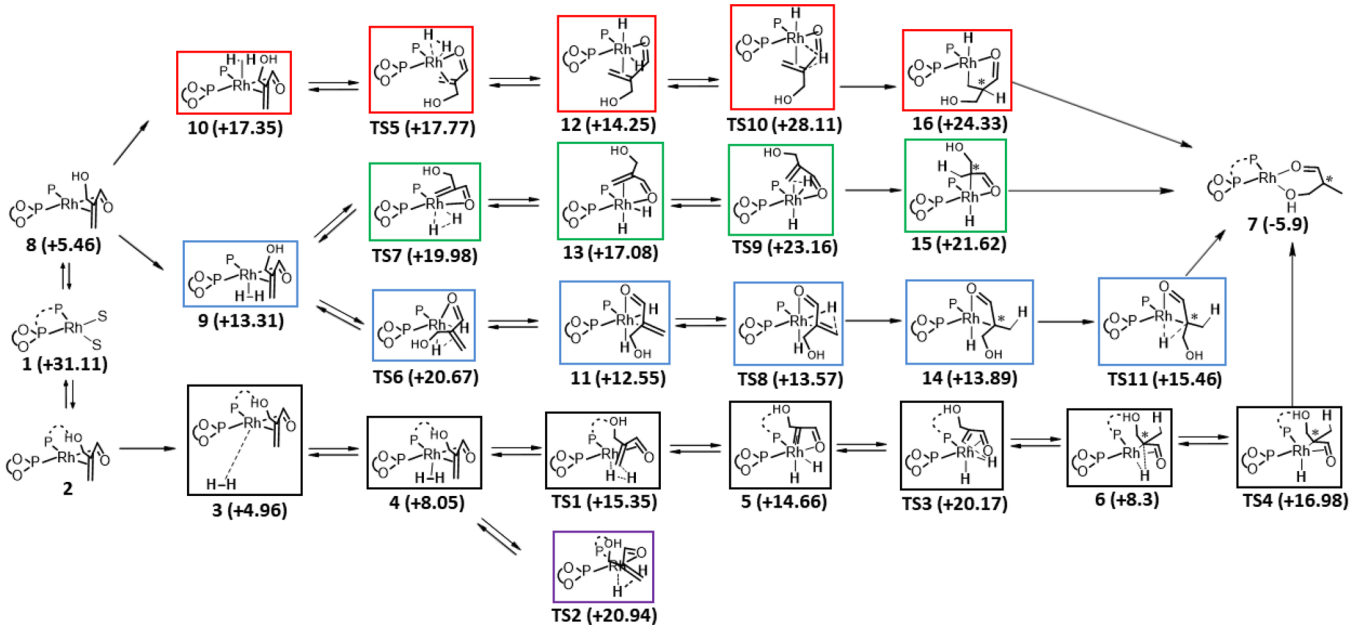

Figure 14. Structures of the intermediates and transition states stemming from the pro-*S* diastereomers **2** and **8**. In between brackets are indicated the relative free energies of the transition states and intermediates in kcal mol^{-1} at 298 K. These were calculated on the basis of the energy of structure **2** (catalyst–substrate adduct with hydrogen bond).

DOI: 10.1021/acscatal.9b01809
ACS Catal. 2019, 9, 7535–7547

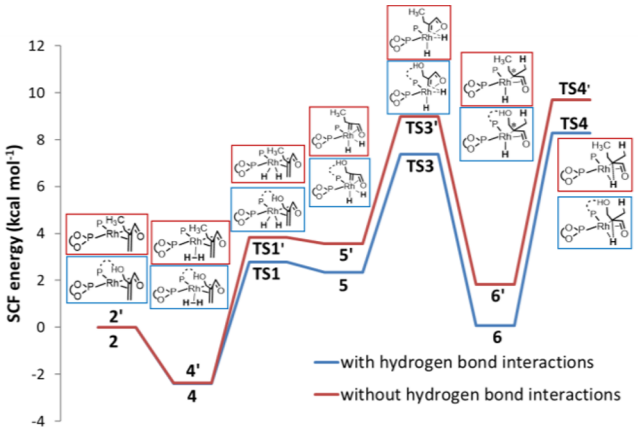

Figure 15. Relative SCF energies of the reaction with and without hydrogen bond interaction between the catalyst and the substrate; **2** and **2′** are set to zero.

hydrogen complexes (**9** and **10**), the transition states of the oxidative addition step (**TS5**, **TS6**, and **TS7**), the dihydride octahedral complexes (**11**, **12**, and **13**), the transition states of the hydride migration step (**TS8**, **TS9**, and **TS10**), the alkylhydride species (**14**, **15**, and **16**), and the reductive elimination step **TS11**. For all of these calculated pathways, only one path is competitive with the pathway with the interactions between the substrate and the catalyst (blue path in Figure 14). Under standard conditions (i.e., 10 bar of H_2, room temperature), the thermodynamic catalyst−substrate complex **2** is formed rapidly, leading to only one major species in solution (as could be observed by NMR experiments). Complex **2** is the resting state, and the non-H-bond path is accessible only via intermediate **8**.[108] Therefore, the feasibilities of the different pathways must all be compared on the basis of the energy barriers relative to the energy of complex **2**, which is the TOF-determining intermediate (TDI). This result is in agreement with the experimental data that assigned diastereomer **2** as being the resting state of the reaction (NMR experiments). The H-bond path (black path in Figure 14) has similar energy transition states as compared to one path in which no hydrogen bond is present (blue path in Figure 14). Therefore, both paths are preferred, and the H-bond path is involved in producing the *S*-product. The overall energy barrier is represented by the hydride migration step **TS3** (as well as **TS6**, which has a similar energy), i.e., the TOF-determining transition state (TDTS).

To evaluate the importance of the H-bond effect in the preferred unsaturated pathway (black pathway, Figure 14), we removed the hydrogen bond interactions in the structures **2**, **4**, **5**, and **6** and the transition states **TS1**, **TS3**, and **TS4** by replacing the hydroxyl group on the substrate by a hydrogen. The SCF energies of the structures were plotted on the same energy profile, taking the energy of the diastereomers **2** (or **2′**) as a reference. As can be seen from Figure 15 the hydrogen bond interaction is responsible for the stabilization of the reaction path by approximately 2 kcal mol^{-1}, compared to the structures not featuring hydrogen bonds between the catalyst and the substrate. These results reflect the role of the H-bond, as without this extra transition state stabilization, the alternative routes become competitive leading to lower selectivity.

Origin of the Selectivity. The influence of the hydrogen bond between the substrate and the catalyst affects the enantioselectivity of the reaction, which was further investigated by computing the competing pathways starting from the pro-*R* diastereomer of lowest energy (structure **31**, Figure

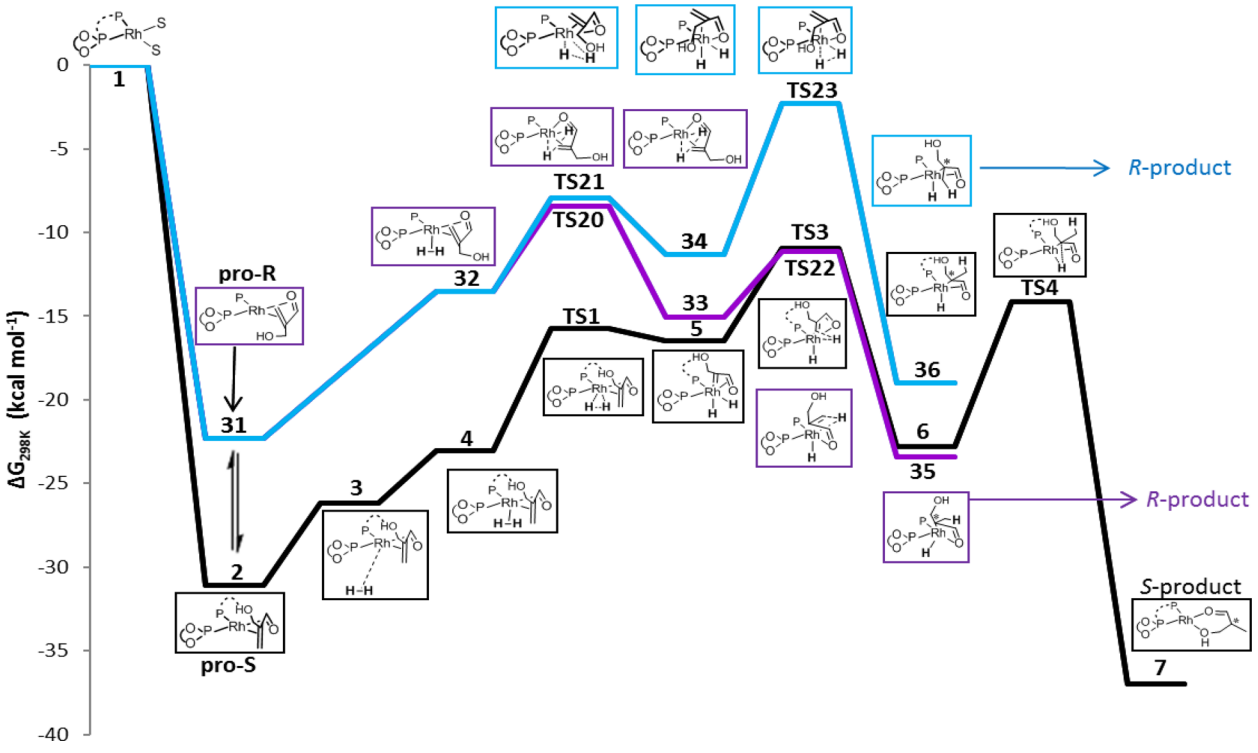

Figure 16. Energy profile of the unsaturated pathways from the pro-*S* diastereoisomer and the pro-*R* diastereoisomer (free energies at 298 K in kcal mol^{-1}).

DOI: 10.1021/acscatal.9b01809
ACS Catal. 2019, 9, 7535−7547

16). The approach and coordination of molecular hydrogen from the lower face of the catalysts is favored as compared to the upper face since the interactions between the two ligands block the approach from the upper face (structure **32**, Figure 16). Upon oxidative addition of hydrogen at **32**, the substrate can rotate in two directions leading to two different dihydride octahedral complexes (structures **33** and **34**). This step occurs for both ways with a close energy barrier (**TS20** and **TS21**). After the oxidative addition step, structure **34** (pro-*R*) undergoes hydride migration with a high energy barrier (**TS23**), making this path energetically unfavorable. For the formation of the *R*-product, the pathway via **TS20** is also available, and this is lower in energy. For the formation of the *S*-product the path via **TS3** is the lowest in energy. As this is the lowest energy pathway available from resting state complex **2** (which is supported by NMR experiments), these calculations are in line with the preferential formation of the *S*-product observed experimentally (black path).[109] The method of calculation used is probably not accurate enough for quantitative analysis of the calculated enantioselectivity.

SUMMARY AND CONCLUSION

The characterization of the precatalyst and solvate species revealed a hydrogen bond between the two ligands. Upon coordination of a substrate functionalized with a H-bond donor, the catalyst modifies its conformation to establish hydrogen bonds with the substrate. The hydroxyl group of the substrate is inserted in the hydrogen bond between the two ligands giving a total of two hydrogen bonds, leading to a high stabilization of the diastereomeric complex **3a**. This complex could be observed during catalysis under standard conditions by *in situ* NMR and therefore is most likely the resting state of the reaction. Upon hydrogenation of diastereomer **3a**, no other intermediates could be detected. The product of the reaction is obtained with 98% enantiomeric excess. All the experiments performed on the mechanism of hydrogenation of substrate **S3** are in line with a lock-and-key mechanism in which several hydrogen bonds are involved in the stabilization of different intermediates along the reaction mechanism. The in-depth study of the mechanism of hydrogenation of substrate **S4** (the substrate that lacks the hydrogen bond donor group) showed that this substrate follows also a lock-and-key mechanism, but in this reaction pathway no hydrogen bonds between the catalyst and the substrate are formed. As a result, this substrate is hydrogenated with lower rates. Also, the dependency of the selectivity on the hydrogen pressure for substrate **S4** (Figure 8) indicates that both substrates follow a lock-and-key mechanism, in which the hydrogenation of substrate **S4** is more sensitive to the hydrogen pressure due to the lack of H-bond effect during the reaction. Additionally, the hydrogen bonds set up between the catalyst and the substrate lead to high enantioselectivity by providing for the discrimination of the prochiral faces of the coordinated alkene in the pro-*R* and pro-*S* diastereoisomers, as was demonstrated by DFT. Importantly, this work shows that supramolecular interactions between the substrate and the functional groups of the catalyst influence the activity and the selectivity of the rhodium-catalyzed asymmetric hydrogenation reaction. Understanding this in detail now sets the stage for implementation of such strategies in the rational design of new supramolecular catalysts.

ASSOCIATED CONTENT

Supporting Information

The Supporting Information is available free of charge on the ACS Publications website at DOI: 10.1021/acscatal.9b01809.

Experimental details and additional figures including NMR spectra and structures (PDF)

Crystallographic information file for **1**−**3** (CIF)

AUTHOR INFORMATION

Corresponding Author

*E-mail: j.n.h.reek@uva.nl.

ORCID

Bas de Bruin: 0000-0002-3482-7669

Joost N. H. Reek: 0000-0001-5024-508X

Notes

The authors declare no competing financial interest.

ACKNOWLEDGMENTS

We would like to thank Sergio Dominguez for his contribution to the VCD analysis.

REFERENCES

(1) Johnson, N. B.; Lennon, I. C.; Moran, P. H.; Ramsden, J. A. Industrial-Scale Synthesis and Applications of Asymmetric Hydrogenation Catalysts. *Acc. Chem. Res.* **2007**, *40* (12), 1291−1299.

(2) Shimizu, H.; Nagasaki, I.; Matsumura, K.; Sayo, N.; Saito, T. Developments in Asymmetric Hydrogenation from an Industrial Perspective. *Acc. Chem. Res.* **2007**, *40* (12), 1385−1393.

(3) Saudan, L. A. Hydrogenation Processes in the Synthesis of Perfumery Ingredients. *Acc. Chem. Res.* **2007**, *40* (12), 1309−1319.

(4) Ager, D. J.; de Vries, H. M.; de Vries, J. G. Asymmetric Homogeneous Hydrogenations at Scale. *Chem. Soc. Rev.* **2012**, *41*, 3340−3380.

(5) Etayo, P.; Vidal-Ferran, A. Rhodium-Catalysed Asymmetric Hydrogenation as a Valuable Synthetic Tool for the Preparation of Chiral Drugs. *Chem. Soc. Rev.* **2013**, *42* (2), 728−754.

(6) Blaser, H.-U.; Malan, C.; Pugin, B.; Spindler, F.; Steiner, H.; Studer, M. Selective Hydrogenation for Fine Chemicals: Recent Trends and New Developments. *Adv. Synth. Catal.* **2003**, *345* (12), 103−151.

(7) Seo, C. S. G.; Morris, R. H. Catalytic Homogeneous Asymmetric Hydrogenation: Successes and Opportunities. *Organometallics* **2019**, *38* (1), 47−65.

(8) Blaser, H.; Pugin, B.; Spindler, F. Progress in Enantioselective Catalysis Assessed from an Industrial Point of View. *J. Mol. Catal. A: Chem.* **2005**, *231* (1−2), 1−20.

(9) Horner, L.; Siegel, H.; Büthe, H. Asymmetric Catalytic Hydrogenation with an Optically Active Phosphinerhodium Complex in Homogeneous Solution. *Angew. Chem., Int. Ed. Engl.* **1968**, *7* (12), 942−942.

(10) Knowles, W. S.; Sabacky, M. J. Catalytic Asymmetric Hydrogenation Employing a Soluble, Optically Active, Rhodium Complex. *Chem. Commun.* **1968**, No. 22, 1445.

(11) Dang, T. P.; Kagan, H. B. The Asymmetric Synthesis of Hydratropic Acid and Amino-Acids by Homogeneous Catalytic Hydrogenation. *J. Chem. Soc. D* **1971**, *7* (10), 481.

(12) Knowles, W. S.; Sabacky, M. J.; Vineyard, B. D.; Weinkauff, D. J. Asymmetric Hydrogenation with a Complex of Rhodium and a Chiral Bisphosphine. *J. Am. Chem. Soc.* **1975**, *97* (9), 2567−2568.

(13) Knowles, W. S. Asymmetric Hydrogenations (Nobel Lecture) Copyright© The Nobel Foundation 2002. We Thank the Nobel Foundation, Stockholm, for Permission to Print This Lecture. *Angew. Chem., Int. Ed.* **2002**, *41* (12), 1998.

DOI: 10.1021/acscatal.9b01809
ACS Catal. 2019, 9, 7535−7547

(14) Tang, W.; Zhang, X. New Chiral Phosphorus Ligands for Enantioselective Hydrogenation. *Chem. Rev.* **2003**, *103* (8), 3029−3070.
(15) Jäkel, C.; Paciello, R. High-Throughput and Parallel Screening Methods in Asymmetric Hydrogenation. *Chem. Rev.* **2006**, *106* (7), 2912−2942.
(16) Chiba, M.; Takahashi, H.; Takahashi, H.; Morimoto, T.; Achiwa, K. Synthesis and Application of a Novel Bisphosphine Ligand, (−)-DIOCP, as an Unsymmetrized Diop to Prove the General Utility of New Designing Concept. *Tetrahedron Lett.* **1987**, *28* (32), 3675−3678.
(17) Takahashi, H.; Morimoto, T.; Achiwa, K. Highly Effective Catalytic Asymmetric Hydrogenations of α-Keto Esters and an α-Keto Acetal with New Neutral Chiral Pyrrolidinebisphosphine-Rhodium Complexes. *Chem. Lett.* **1987**, *16* (5), 855−858.
(18) Togni, A.; Breutel, C.; Schnyder, A.; Spindler, F.; Landert, H.; Tijani, A. A Novel Easily Accessible Chiral Ferrocenyldiphosphine for Highly Enantioselective Hydrogenation, Allylic Alkylation, and Hydroboration Reactions. *J. Am. Chem. Soc.* **1994**, *116* (9), 4062−4066.
(19) Holz, J.; Heller, D.; Stürmer, R.; Börner, A. Synthesis of the First Water-Soluble Chiral Tetrahydroxy Diphosphine Rh(I) Catalyst for Enantioselective Hydrogenation. *Tetrahedron Lett.* **1999**, *40* (39), 7059−7062.
(20) Yoon, T. P.; Jacobsen, E. N. Privileged Chiral Catalysts. *Science* **2003**, *299* (5613), 1691−1693.
(21) Imamoto, T.; Tamura, K.; Zhang, Z.; Horiuchi, Y.; Sugiya, M.; Yoshida, K.; Yanagisawa, A.; Gridnev, I. D. Rigid P-Chiral Phosphine Ligands with Tert-Butylmethylphosphino Groups for Rhodium-Catalyzed Asymmetric Hydrogenation of Functionalized Alkenes. *J. Am. Chem. Soc.* **2012**, *134*, 1754.
(22) Noyori, R. Asymmetric Catalysis: Science and Opportunities (Nobel Lecture). *Angew. Chem., Int. Ed.* **2002**, *41* (12), 2008−2022.
(23) Reetz, M. T. T.; Mehler, G. Highly Enantioselective Rh-Catalyzed Hydrogenation Reactions Based on Chiral Monophosphite Ligands. *Angew. Chem., Int. Ed.* **2000**, *39* (21), 3889−3890.
(24) Reetz, M. T.; Sell, T.; Meiswinkel, A.; Mehler, G. A New Principle in Combinatorial Asymmetric Transition-Metal Catalysis: Mixtures of Chiral Monodentate P Ligands. *Angew. Chem., Int. Ed.* **2003**, *42* (7), 790−793.
(25) Hua, Z.; Vassar, V. C.; Ojima, I. Synthesis of New Chiral Monodentate Phosphite Ligands and Their Use in Catalytic Asymmetric Hydrogenation. *Org. Lett.* **2003**, *5* (21), 3831−3834.
(26) Reetz, M. T.; Sell, T. Rhodium-Catalyzed Enantioselective Hydrogenation Using Chiral Monophosphonite Ligands. *Tetrahedron Lett.* **2000**, *41* (33), 6333−6336.
(27) Gillon, A.; Heslop, K.; Hyett, D. J.; Martorell, A.; Orpen, A. G.; Pringle, P. G.; Claver, C.; Fernandez, E. Biarylphosphonites: A Class of Monodentate Phosphorus(Iii) Ligands That Outperform Their Chelating Analogues in Asymmetric Hydrogenation Catalysis. *Chem. Commun.* **2000**, *0* (11), 961−962.
(28) van den Berg, M.; Minnaard, A. J.; Schudde, E. P.; van Esch, J.; de Vries, A. H. M.; de Vries, J. G.; Feringa, B. L. Highly Enantioselective Rhodium-Catalyzed Hydrogenation with Monodentate Ligands. *J. Am. Chem. Soc.* **2000**, *122* (46), 11539−11540.
(29) Peña, D.; Minnaard, A. J.; de Vries, J. G.; Feringa, B. L.; et al. Highly Enantioselective Rhodium-Catalyzed Hydrogenation of β-Dehydroamino Acid Derivatives Using Monodentate Phosphoramidites. *J. Am. Chem. Soc.* **2002**, *124* (49), 14552−14553.
(30) Hu, A.-G.; Fu, Y.; Xie, J.; Zhou, H.; Wang, L.-X.; Zhou, Q.-L. Monodentate Chiral Spiro Phosphoramidites: Efficient Ligands for Rhodium-Catalyzed Enantioselective Hydrogenation of Enamides. *Angew. Chem., Int. Ed.* **2002**, *41* (13), 2348−2350.
(31) Teichert, J. F.; Feringa, B. L. *Angew. Chem., Int. Ed.* **2010**, *49*, 2486−2528.
(32) Jerphagnon, T.; Renaud, J.-L.; Bruneau, C. Chiral Monodentate Phosphorus Ligands for Rhodium-Catalyzed Asymmetric Hydrogenation. *Tetrahedron: Asymmetry* **2004**, *15* (14), 2101−2111.
(33) GUO, H. Recent Advances in Catalytic Asymmetric Hydrogenation: Renaissance of the Monoden-Tate Phosphorus Ligands. *Chin. Sci. Bull.* **2004**, *49* (19), 2003.
(34) Reetz, M. T.; Meiswinkel, A.; Mehler, G.; Angermund, K.; Graf, M.; Thiel, W.; Mynott, R.; Blackmond, D. G. Why Are BINOL-Based Monophosphites Such Efficient Ligands in Rh-Catalyzed Asymmetric Olefin Hydrogenation? *J. Am. Chem. Soc.* **2005**, *127* (29), 10305−10313.
(35) Brown, J. M.; Chaloner, P. A. Mechanism of Asymmetric Hydrogenation Catalysed by Rhodium(I)Trans-4,5-Bis-(Diphenylphosphinomethyl)-2,2-Dimethyldioxolan (DIOP) Complexes. *J. Chem. Soc., Chem. Commun.* **1978**, No. 7, 321.
(36) Brown, J. M.; Chaloner, P. A. THE MECHANISM OF ASYMMETRIC HYDROGENATION CATALYSED BY RHODIUM (I) DIPAMP COMPLEXES. *Tetrahedron Lett.* **1978**, *19*, 1877.
(37) Brown, J. M.; Chaloner, P. A. Asymmetric Homogeneous Hydrogenation Catalysed by Rhodium Complexes; the Binding Modes of Enamides Defined by 13C n.m.r. Spectroscopy. *J. Chem. Soc., Chem. Commun.* **1979**, No. 14, 613.
(38) Brown, J. M.; Chaloner, P. A. Structural Characterisation of a Transient Intermediate in Rhodium-Catalysed Asymmetric Homogeneous Hydrogenation. *J. Chem. Soc., Chem. Commun.* **1980**, No. 8, 344.
(39) brown, J. M.; Chaloner, P. A.; Glaser, R.; Geresh, S. Intermediates in Asymmetric Hydrogenation. *Tetrahedron* **1980**, *36* (6), 815−825.
(40) Halpern, J.; Riley, D. P.; Chan, A. S. C.; Pluth, J. J. Novel Coordination Chemistry and Catalytic Properties of Cationic 1,2-Bis(Diphenylphosphino)Ethanerhodium(I) Complexes. *J. Am. Chem. Soc.* **1977**, *99* (24), 8055−8057.
(41) Chan, A. S. C.; Pluth, J. J.; Halpern, J. Identification of the Enantioselective Step in the Asymmetric Catalytic Hydrogenation of a Prochiral Olefin. *J. Am. Chem. Soc.* **1980**, *102* (18), 5952−5954.
(42) Chan, A. S. C.; Halpern, J. Interception and Characterization of a Hydridoalkylrhodium Intermediate in a Homogeneous Catalytic Hydrogenation Reaction. *J. Am. Chem. Soc.* **1980**, *102* (2), 838−840.
(43) Halpern, J. Mechanism and Stereoselectivity of Asymmetric Hydrogenation. *Science (Washington, DC, U. S.)* **1982**, *217* (4558), 401−407.
(44) Landis, C. R.; Halpern, J. Asymmetric hydrogenation of methyl (Z)-a-acetamidocinnamate catalyzed by [1,2-bis(phenyl-o-anisoyl)-phosphino)ethane]rhodium(I): kinetics, mechanism and origin of enantioselection. *J. Am. Chem. Soc.* **1987**, *109* (6), 1746−1754.
(45) Landis, C. R.; Hilfenhaus, P.; Feldgus, S. Structures and Reaction Pathways in Rhodium(I)-Catalyzed Hydrogenation of Enamides: A Model DFT Study. *J. Am. Chem. Soc.* **1999**, *121* (38), 8741−8754.
(46) Feldgus, S.; Landis, C. R.; June, R. V. Large-Scale Computational Modeling of [Rh (DuPHOS)] + -Catalyzed Hydrogenation of Prochiral Enamides : Reaction Pathways and the Origin of Enantioselection. *J. Am. Chem. Soc.* **2000**, *122* (51), 12714−12727.
(47) Marinetti, A.; Jus, S.; Genêt, J.-P. Investigation into an Asymmetric Hydrogenation Promoted by Rhodium-Phosphetane Complexes. *Tetrahedron Lett.* **1999**, *40* (48), 8365−8368.
(48) Evans, D. A.; Michael, F. E.; Tedrow, J. S.; Campos, K. R. *J. Am. Chem. Soc.* **2003**, *125*, 3534−3543.
(49) Wassenaar, J.; Reek, J. N. H. INDOLPhos: Novel Hybrid Phosphine-Phosphoramidite Ligands for Asymmetric Hydrogenation and Hydroformylation. *Dalt. Trans.* **2007**, *0* (34), 3750.
(50) Wassenaar, J.; Kuil, M.; Lutz, M.; Spek, A. L. L.; Reek, J. N. H. N. H. Asymmetric Hydrogenation with Highly Active IndolPhos-Rh Catalysts: Kinetics and Reaction Mechanism. *Chem. - Eur. J.* **2010**, *16* (22), 6509−6517.
(51) Pullmann, T.; Engendahl, B.; Zhang, Z.; Hölscher, M.; Zanotti-Gerosa, A.; Dyke, A.; Franciò, G.; Leitner, W. Quinaphos and Dihydro-Quinaphos Phosphine-Phosphoramidite Ligands for Asymmetric Hydrogenation. *Chem. - Eur. J.* **2010**, *16* (25), 7517−7526.

DOI: 10.1021/acscatal.9b01809
ACS Catal. 2019, 9, 7535−7547

(52) Hammerer, T.; Leitner, W.; Franciò, G. Synthesis of Phospholane-Phosphoramidite Ligands and Their Application in Asymmetric Catalysis. *ChemCatChem* **2015**, *7* (10), 1583−1592.
(53) Schmitz, C.; Holthusen, K.; Leitner, W.; Franciò, G. Bidentate Phosphine-Phosphoramidite Ligands of the BettiPhos Family for Rh-Catalyzed Asymmetric Hydrogenation. *Eur. J. Org. Chem.* **2017**, *2017* (28), 4111−4116.
(54) Gridnev, I. D.; Higashi, N.; Asakura, K.; Imamoto, T. Mechanism of Asymmetric Hydrogenation Catalyzed by a Rhodium Complex of (S,S)-1,2-Bis(Tert -Butylmethylphosphino)Ethane. Dihydride Mechanism of Asymmetric Hydrogenation. *J. Am. Chem. Soc.* **2000**, *122* (30), 7183−7194.
(55) Gridnev, I. D.; Yasutake, M.; Higashi, N.; Imamoto, T. Asymmetric Hydrogenation of Enamides with Rh-BisP* and Rh-MiniPHOS Catalysts. Scope, Limitations, and Mechanism. *J. Am. Chem. Soc.* **2001**, *123* (22), 5268−5276.
(56) Imamoto, T.; Itoh, T.; Yoshida, K.; Gridnev, I. D. D. Marked Deuterium Isotope Effects on the Enantioselectivity in Rhodium-Catalyzed Asymmetric Hydrogenation of Enamides. *Chem. - Asian J.* **2008**, *3* (8−9), 1636−1641.
(57) Gridnev, I. D.; Imamoto, T.; Hoge, G.; Kouchi, M.; Takahashi, H. Asymmetric Hydrogenation Catalyzed by a Rhodium Complex of (R)-(Tert -Butylmethylphosphino)(Di- Tert -Butylphosphino)-Methane: Scope of Enantioselectivity and Mechanistic Study. *J. Am. Chem. Soc.* **2008**, *130* (8), 2560−2572.
(58) Gridnev, I. D.; Kohrt, C.; Liu, Y. Direct Experimental and Computational Evidence for the Dihydride Pathway in TangPHOS-Rh Catalysed Asymmetric Hydrogenation. *Dalt. Trans.* **2014**, *43* (4), 1785−1790.
(59) Gridnev, I. D.; Imamoto, T. Mechanism of Enantioselection in Rh-Catalyzed Asymmetric Hydrogenation. The Origin of Utmost Catalytic Performance. *Chem. Commun.* **2009**, *0* (48), 7447.
(60) Hansen, E.; Rosales, A. R.; Tutkowski, B.; Norrby, P.-O.; Wiest, O. Prediction of Stereochemistry Using Q2MM. *Acc. Chem. Res.* **2016**, *49* (5), 996−1005.
(61) Rosales, A. R.; Wahlers, J.; Limé, E.; Meadows, R. E.; Leslie, K. W.; Savin, R.; Bell, F.; Hansen, E.; Helquist, P.; Munday, R. H.; et al. Rapid Virtual Screening of Enantioselective Catalysts Using CatVS. *Nat. Catal.* **2019**, *2* (1), 41−45.
(62) Reid, J. P.; Sigman, M. S. Comparing Quantitative Prediction Methods for the Discovery of Small-Molecule Chiral Catalysts. *Nat. Rev. Chem.* **2018**, *2* (10), 290−305.
(63) Guan, Y.; Wheeler, S. E. Automated Quantum Mechanical Predictions of Enantioselectivity in a Rhodium-Catalyzed Asymmetric Hydrogenation. *Angew. Chem., Int. Ed.* **2017**, *56* (31), 9101−9105.
(64) Reetz, M. T.; Mehler, G. Mixtures of Chiral and Achiral Monodentate Ligands in Asymmetric Rh-Catalyzed Olefin Hydrogenation: Reversal of Enantioselectivity. *Tetrahedron Lett.* **2003**, *44* (24), 4593−4596.
(65) Reetz, M. T.; Bondarev, O. Mixtures of Chiral Phosphorous acid Diesters and Achiral P Ligands in the Enantio- and Diastereoselective Hydrogenation of Ketimines. *Angew. Chem., Int. Ed.* **2007**, *46* (24), 4523−4526.
(66) Reetz, M. T.; Guo, H. Mixtures of Monodentate P-Ligands as a Means to Control the Diastereoselectivity in Rh-Catalyzed Hydrogenation of Chiral Alkenes. *Beilstein J. Org. Chem.* **2005**, *6*, 2−7.
(67) Reetz, M. T.; Fu, Y.; Meiswinkel, A. Nonlinear Effects in Rh-Catalyzed Asymmetric Olefin Hydrogenation Using Mixtures of Chiral Monodentate P Ligands. *Angew. Chem., Int. Ed.* **2006**, *45* (9), 1412−1415.
(68) Renom-Carrasco, M.; Lefort, L. Ligand Libraries for High Throughput Screening of Homogeneous Catalysts. *Chem. Soc. Rev.* **2018**, *47* (13), 5038−5060.
(69) Wilkinson, M. J.; van Leeuwen, P. W. N. M.; Reek, J. N. H. New Directions in Supramolecular Transition Metal Catalysis. *Org. Biomol. Chem.* **2005**, *3* (13), 2371.
(70) Breit, B. Supramolecular Approaches to Generate Libraries of Chelating Bidentate Ligands for Homogeneous Catalysis. *Angew. Chem., Int. Ed.* **2005**, *44* (42), 6816−6825.
(71) Sandee, A. J.; van der Burg, A. M.; Reek, J. N. H. UREAphos: Supramolecular Bidentate Ligands for Asymmetric Hydrogenation. *Chem. Commun.* **2007**, *0* (8), 864−866.
(72) Wieland, J.; Breit, B. A Combinatorial Approach to the Identification of Self-Assembled Ligands for Rhodium-Catalysed Asymmetric Hydrogenation. *Nat. Chem.* **2010**, *2* (10), 832−837.
(73) Sandee, A. J.; Reek, J. N. H. Bidentate Ligands by Supramolecular Chemistry—the Future for Catalysis? *Dalt. Trans.* **2006**, *0* (28), 3385−3391.
(74) Pignataro, L.; Carboni, S.; Civera, M.; Colombo, R.; Piarulli, U.; Gennari, C. PhthalaPhos: Chiral Supramolecular Ligands for Enantioselective Rhodium-Catalyzed Hydrogenation Reactions. *Angew. Chem., Int. Ed.* **2010**, *49* (37), 6633−6637.
(75) Pignataro, L.; Boghi, M.; Civera, M.; Carboni, S.; Piarulli, U.; Gennari, C. Rhodium-Catalyzed Asymmetric Hydrogenation of Olefins with PhthalaPhos, a New Class of Chiral Supramolecular Ligands. *Chem. - Eur. J.* **2012**, *18* (5), 1383−1400.
(76) Raynal, M.; Ballester, P.; Vidal-Ferran, A.; Van Leeuwen, P. W. N. M. Supramolecular Catalysis. Part 1: Non-Covalent Interactions as a Tool for Building and Modifying Homogeneous Catalysts. *Chem. Soc. Rev.* **2014**, *43* (5), 1660−1733.
(77) Mote, N. R.; Chikkali, S. H. Hydrogen-Bonding-Assisted Supramolecular Metal Catalysis. *Chem. - Asian J.* **2018**, *13* (23), 3623−3646.
(78) Gulyás, H.; Benet-Buchholz, J.; Escudero-Adan, E. C.; Freixa, Z.; van Leeuwen, P. W. N. M. Ionic Interaction as a Powerful Driving Force for the Formation of Heterobidentate Assembly Ligands. *Chem. - Eur. J.* **2007**, *13* (12), 3424−3430.
(79) Jiang, X.; Lefort, L.; Goudriaan, P. E.; de Vries, A. H. M.; van Leeuwen, P. W. N. M.; de Vries, J. G.; Reek, J. N. H. Screening of a Supramolecular Catalyst Library in the Search for Selective Catalysts for the Asymmetric Hydrogenation of a Difficult Enamide Substrate. *Angew. Chem., Int. Ed.* **2006**, *45* (8), 1223−1227.
(80) Birkholz, M.-N.; Dubrovina, N. V.; Jiao, H.; Michalik, D.; Holz, J.; Paciello, R.; Breit, B.; Börner, A. Enantioselective Hydrogenation with Self-Assembling Rhodium Phosphane Catalysts: Influence of Ligand Structure and Solvent. *Chem. - Eur. J.* **2007**, *13* (20), 5896−5907.
(81) Chen, W.; McCormack, P. J.; Mohammed, K.; Mbafor, W.; Roberts, S. M.; Whittall, J. Stereoselective Synthesis of Ferrocene-BasedC2-Symmetric Diphosphine Ligands: Application to the Highly Enantioselective Hydrogenation of α-Substituted Cinnamic Acids. *Angew. Chem., Int. Ed.* **2007**, *46* (22), 4141−4144.
(82) Šmejkal, T.; Breit, B. A Supramolecular Catalyst for Regioselective Hydroformylation of Unsaturated Carboxylic Acids. *Angew. Chem., Int. Ed.* **2008**, *47* (2), 311−315.
(83) Dydio, P.; Rubay, C.; Gadzikwa, T.; Lutz, M.; Reek, J. N. H. Cofactor"-Controlled Enantioselective Catalysis. *J. Am. Chem. Soc.* **2011**, *133* (43), 17176−17179.
(84) Wang, Q.; Liu, X. X.; Liu, X. X.; Li, B.; Nie, H.; Zhang, S.; Chen, W. Highly Enantioselective Hydrogenation of 2-Substituted-2-Alkenols Catalysed by a ChenPhos−Rh Complex. *Chem. Commun.* **2014**, *50* (8), 978−980.
(85) Yamagishi, T.; Yatagai, M. Efficient 1.4-Asymmetric Induction Utilizing Electrostatic Interaction between Ligand and Substrate in the Asymmetric Hydrogenation of Didehydrodipeptides. *J. Chem. Soc., Perkin Trans. 1* **1988**, No. 7, 1787−1790.
(86) Ikeda, S.; Yamagishi, T.; Yamaguchi, M.; Hida, M. Effects of Solvent and Temperature on the 1,4-Asymmetric Induction in the Diastereoselective Hydrogenation of Dehydrodipeptides. *Bull. Chem. Soc. Jpn.* **1989**, *62* (11), 3508−3512.
(87) Sawamura, M.; Ito, Y. Catalytic Asymmetric Synthesis by Means of Secondary Interaction between Chiral Ligands and Substrates. *Chem. Rev.* **1992**, *92* (5), 857−871.
(88) Börner, A. Biomimetic Asymmetric Hydrogenation. *Chirality* **2001**, *13* (10), 625−628.
(89) Breuil, P.-A. R.; Patureau, F. W.; Reek, J. N. H. Singly Hydrogen Bonded Supramolecular Ligands for Highly Selective

DOI: 10.1021/acscatal.9b01809
ACS Catal. 2019, 9, 7535−7547

Rhodium-Catalyzed Hydrogenation Reactions. *Angew. Chem., Int. Ed.* **2009**, *48* (12), 2162−2165.
(90) Li, Q.; Mao, S.; Cui, Y.; Jia, Y. Stereoselective Synthesis of the C 5 − C 18 Fragment of Halichomycin. *J. Org. Chem.* **2012**, *77* (8), 4111−4116.
(91) For a preliminary communication, see: Daubignard, J.; Detz, R. J.; Jans, A. C. H.; de Bruin, B.; Reek, J. N. H. Rational Optimization of Supramolecular Catalysts for the Rhodium-Catalyzed Asymmetric Hydrogenation Reaction. *Angew. Chem., Int. Ed.* **2017**, *56* (42), 13056−13060.
(92) For details, see the Supporting Information.
(93) A complex analogue to **1** but in which no hydrogen bonds can be formed between the two ligands was obtained by mixing 1 equiv of ligand **L1** with 1 equiv of triphenylphosphine and 1 equiv of the $[Rh(cod)_2]BF_4$ salt. The sample was stirred for 1 h under an argon atmosphere, and the ^{31}P NMR spectrum was recorded. A mixture of heterocomplex $Rh(\mathbf{L_1})(PPh_3)$ and homocomplexes (complex $Rh(\mathbf{L_1})_2$ and complex $Rh(PPh3)_2$) was observed. Also, a 2D 1H−1H COSY NMR experiment was performed, revealing that the NH group of the heterocomplex $Rh(\mathbf{L_1})(PPh_3)$ has a chemical shift of δ = 4.29 ppm (for details, see the Supporting Information).
(94) Liu, Y.; Sandoval, C. A.; Yamaguchi, Y.; Zhang, X.; Wang, Z.; Kato, K.; Ding, K. Hydrogen Bonding Makes a Difference in the Rhodium-Catalyzed Enantioselective Hydrogenation Using Monodentate Phosphoramidites. *J. Am. Chem. Soc.* **2006**, *128* (44), 14212−14213.
(95) Other structures featuring hydrogen bond interactions between the substrate and the catalyst (for instance, involving the BINOL group of the phosphoramidite) were calculated, but all of these ones were higher in energy.
(96) Enantiomeric excess was determined by HPLC, and the absolute configuration of the product was determined by VCD spectroscopy (for details, see the experimental sections in the SI).
(97) [cat] = 1 mM, substrate:catalyst = 100:1, 10 bar H_2, r.t., 18 h, CH_2Cl_2.
(98) The absolute configuration of product **5** was determined by analytical derivatization of product P3 (for details, see the experimental sections in the SI).
(99) Gridnev, I. D.; Alberico, E.; Gladiali, S. Captured at Last: A Catalyst−substrate Adduct and a Rh-Dihydride Solvate in the Asymmetric Hydrogenation by a Rh-Monophosphine Catalyst. *Chem. Commun.* **2012**, *48* (16), 2186.
(100) Vineyard, B. D.; Knowles, W. S.; Sabacky, M. J.; Bachman, G. L.; Weinkauff, D. J. Asymmetric Hydrogenation. Rhodium Chiral Bisphosphine Catalyst. *J. Am. Chem. Soc.* **1977**, *99* (18), 5946−5952.
(101) Landis, C. R.; Halpern, J. Asymmetric Hydrogenation of Methyl (Z)-.Alpha.-Acetamidocinnamate Catalyzed by [1,2-Bis-(Phenyl-o-Anisoyl)Phosphino)Ethane]Rhodium(I): Kinetics, Mechanism and Origin of Enantioselection. *J. Am. Chem. Soc.* **1987**, *109* (6), 1746−1754.
(102) Schmidt, T.; Dai, Z.; Drexler, H. H.; Hapke, M.; Preetz, A.; Heller, D. The Major/Minor Concept: Dependence of the Selectivity of Homogeneously Catalyzed Reactions on Reactivity Ratio and Concentration Ratio of the Intermediates. *Chem. - Asian J.* **2008**, *3* (7), 1170−1180.
(103) Drommi, D.; Micalizzi, G.; Arena, C. G. New Chiral Diphosphoramidite Rhodium(I) Complexes for Asymmetric Hydrogenation. *Appl. Organomet. Chem.* **2014**, *28* (8), 614−619.
(104) Aloui, A.; Delbecq, F.; Sautet, P.; De Bellefon, C. Further Insight in the Minor/Major Concept Using Hydrogen Pressure Effect in Asymmetric Hydrogenation. *J. Mol. Catal. A: Chem.* **2012**, *363−364*, 214−222.
(105) *In situ* HP NMR identified the catalyst−substrate complex **3a** as the only observable species in solution during catalysis (for details, see the Supporting Information). However, we cannot conclude unequivocally that the diastereomer **3a** is the resting state of the catalysis since the solvate complex **2** cannot be properly detected in the ^{31}P NMR spectrum during the catalysis
(106) We performed the same series of experiments for substrate **S5** to study the steric effect of the substituent placed in *cis* position of the phenyl group. The gas-uptake experiments revealed that substrate **S5** is hydrogenated with very low rates (TOF = 5 mol mol^{-1} h^{-1} at 15% conversion [Rh] = 1 mM).
(107) Dydio, P.; Detz, R. J.; Reek, J. N. H. Precise Supramolecular Control of Selectivity in the Rh-Catalyzed Hydroformylation of Terminal and Internal Alkenes. *J. Am. Chem. Soc.* **2013**, *135* (29), 10817−10828.
(108) We could not compute the energy profile for the opening of the secondary interactions between complex **2** and **8**. However, breaking the hydrogen bonds must involve only a small structural change and requires an amount of energy corresponding to two hydrogen bonds (estimated to 5 kcal mol^{-1}); then, the two isomers are in fast equilibrium.
(109) We wanted to evaluate the energy of interconversion between the diastereomers **2** and **31**. Many attempts have been made to compute the coordination of the double bond in the nonchelating species pro-*R* and pro-*S* (even when simulating a dissociative process of the DCM molecule), but no real transition states could be found. The literature reported energetic barriers for the coordination of the double bond in the nonchelating species ranging between 4.9 and 23.1 kcal mol^{-1}. These values hold for the coordination of strong coordinating substrates and in methanol, and therefore the energy of interconversion is expected to be much lower in weak coordinating solvent. According to our energy profile, the hydrogenation of the pro-*R* diastereomer would involve an energy barrier of 14 kcal mol^{-1}. In light of the values reported in the literature and the weak coordination of the DCM molecule, the interconversion of the pro-*R* diastereomer into the pro-*S* diastereomer is most likely to be favored compared to the conversion of the pro-*R* diastereomer into the *R*-product.

DOI: 10.1021/acscatal.9b01809
ACS Catal. 2019, 9, 7535−7547